JOURNAL OF Materials CHEMISTRY

Solution processing and crystallization of ferroelectric samarium modified lead titanate thin films

M. Lourdes Calzada,* Rafael Sirera, Jesús Ricote† and Lorena Pardo

Inst. Ciencia de Materiales de Madrid (CSIC), Cantoblanco, 28049—Madrid, Spain

Samarium-doped lead titanate thin films have been prepared by a sol–gel technique. The processing of precursor solutions through two different synthetic routes and containing differing excesses of PbO is described. The films deposited from these solutions are crystallized by thermal treatments at temperatures higher than 550 °C. The crystalline structure, composition and microstructure of the resulting films are studied by grazing incidence X-ray diffraction analysis, energy dispersive spectroscopy, quantitative scanning electron microscopy and transmission electron microscopy. It is observed that the film microstructure and the development of non-ferroelectric phases in these films are influenced by both the solution chemistry and the lead oxide stoichiometry. Preliminary results concerning the ferroelectric behaviour of these films are also given.

$PbTiO_3$ is a ferroelectric material with perovskite type structure having one of the highest values of spontaneous polarization. The poling of $PbTiO_3$, in both bulk ceramic and thin film forms, requires the application of high electric fields. One approach to overcome this problem is the partial substitution of Pb for various rare-earth elements which has been shown as an efficient method to lower the coercive field, while maintaining important values of spontaneous polarization. The chemical formula for these materials is $Pb_{1-(3x/2)}Ln_xTiO_3$, where Ln is La, Ce, Pr, Nd, Sm, Eu or Gd.[1]

For $Pb_{0.88}Ln_{0.08}TiO_3$ ceramics it was found that the relationship of the coupling factor to the poling field has noticeable different features for various lanthanides. Particularly, it has been reported that the planar coupling factor, K_p, decreases gradually with an increase in the poling field for Ln = Sm. This causes exceptionally enhanced anisotropy in the thickness and planar electromechanical coupling factors of thin ceramic disks, which is interesting for ultrasonic transducers.[2] Surface acoustic wave (SAW) devices employing samarium modified lead titanate ceramics have been developed due to their small temperature coefficient of the SAW coupling factor. Materials with fine grain and low porosity content are required for this practical use, since these properties reduce the SAW propagation losses, increasing the free surface velocity and the surface coupling coefficient.[3–5] Therefore, films of $Pb_{0.88}Sm_{0.08}TiO_3$ could have technological interest for the development of SAW and piezoelectric microdevices.

Processing and properties of lead titanate films modified with lanthanum have been previously reported emphasizing their pyroelectric and electro-optic properties.[6,7] However, to the knowledge of the authors, few attempts to prepare $(Pb,Sm)TiO_3$ thin films have been published,[8,9] despite their potential interest.

Among the different techniques used for the deposition of thin films,[10] the sol–gel method has the advantage of producing homogeneous and uniform layers with an excellent control of the stoichiometry, structure and microstructure.[11] However, it requires the obtention of a stable solution containing all the elements of the composition of the film. Compatibility between multiple metal alkoxides in a multicomponent solution is a problem that sometimes restricts the applicability of sol–gel processing.

Solution chemistry has also been shown to have an effect on the microstructure and electrical properties of the derived films.[12] Studies carried out on several sol–gel-based PZT systems indicate that nanoscale heterogeneities are developed in the solutions during their synthesis. Thin films deposited from these solutions have complex microstructures formed not only by the perovskite phase but also by undesirable second phases.

Phase evolution with temperature for solution derived films proceeds from an amorphous to a pyrochlore phase and from this to a perovskite.[13] During this transformation, loss of lead oxide can be observed. Authors have reported that lead oxide is lost from the intermediate amorphous or pyrochlore phases.[14] Amorphous layers have to contain an appropriate excess of lead oxide to obtain a complete crystallization of the lead based perovskite. Otherwise, residual non-ferroelectric phases will be present in the resulting films.

One of the problems which bring about the preparation of lead titanate films modified with rare-earth cations is the obtention of stable solutions containing the rare-earth element. Here, we discuss our approach to solve this problem for samarium modified lead titanate films. The first part of our investigation has been focussed on the synthesis of stable precipitate-free solutions. Two different processing routes are suggested for the synthesis of these solutions. The resulting microstructures of the polycrystalline thin films deposited from these solutions are compared in order to establish the influence of the processing on the properties of the films.

Experimental

Synthesis of solutions

Two different synthesis routes[15,16] have been used for the preparation of sols of nominal composition $Pb_{0.88}Sm_{0.08}TiO_3$. In one of them [Fig. 1(*a*)] lead acetate trihydrate $Pb(OOCCH_3)_2 \cdot 3H_2O$ (Aldrich), and samarium acetylacetonate $Sm(CH_3COCHCOCH_3)_3$ (Johnson-Matthey), were dissolved in propane-1,3-diol solvent, $HO(CH_2)_3OH$ (Aldrich), and heated under reflux in air for 1 h at 110 °C. After cooling the solution below 70 °C, titanium diisopropoxide bis(acetylacetonate), $Ti(OC_3H_7)_2(CH_3COCHCOCH_3)_2$ (Aldrich) (75 mass% solution in propan-2-ol) was added, using molar ratios of 0.88 : 1, 0.08 : 1 and 5 : 1 of lead to titanium, samarium to titanium and propane-1,3-diol to titanium, respectively. The temperature of the solution was increased to 135 °C and reflux maintained for 8 h to favour reaction of the compounds. Distillation of byproducts yielded a stock solution with a concentration of 1.3 M and a density of 1.4 g cm^{-3}. A 0.5 M

† Current address: Advanced Material Group, Cranfield University, Cranfield, Bedfordshire, UK MK43 0AL.

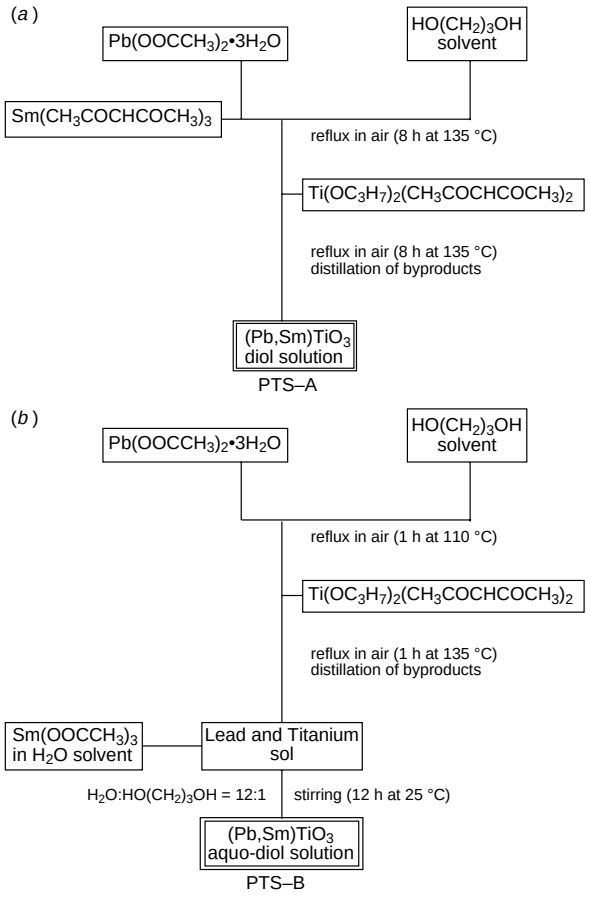

Fig. 1 Synthesis of the solutions (*a*) PTS-A and (*b*) PTS-B

solution was obtained by the dilution of the stock solution with propan-2-ol (Aldrich). This solution is denoted PTS-A.

In the second synthetic route [Fig. 1(*b*)], a lead and titanium sol was first synthesized by heating in propane-1,3-diol, the lead acetate trihydrate and the titanium diisopropoxide bis(acetylacetonate) as described above. Samarium was added to the (Pb,Ti)-sol as a water solution of samarium acetate, $Sm(OOCCH_3)_3$ (Aldrich), with a 12 : 1 molar ratio of water to titanium. After vigorous stirring at room temperature for 12 h, a stable stock solution was obtained with a concentration of 1.2 M and a density of 1.2 g cm^{-3}. Dilution with propan-2-ol led to a 0.5 M solution, denoted as PTS-B. Another two solutions, PTS-B10 and PTS-B20, were synthesized following the scheme of Fig. 1(*b*), but with a 10 and 20 mol% excess of PbO, respectively.

Thermal evolution of the precursor solutions

Thermogravimetry and differential thermal analysis (TGA and DTA) were carried out in air, on dried samples of the solutions, using a rate of 10 °C min^{-1}. The gases removed from the gels during their thermal treatment were studied by evolved gas analysis (EGA), by means of mass spectrometry.

X-Ray diffraction analysis (XRD) was used to study the crystalline structure of the powder obtained after thermal treatment of the solutions.

Thin film preparation

Gel layers were deposited by spin-coating the solutions onto (100)Si substrates at 2000 rpm for 45 s. The silicon wafers were previously sputtered with a *ca.* 500 Å thick adhesion layer of TiO_2 and a Pt electrode of *ca.* 1500 Å thickness.[17,18] The wet films were prefired on a hot plate at 350 °C for 60 s. All the deposition procedures were carried out in a class 100 clean room.

Crystallization was achieved by thermal treatment in air at temperatures >550 °C with soaking times >12 min and heating rates of 10 °C min^{-1} and >500 °C min^{-1}.

Characterisation of the ceramic films

The perovskite structure and second phases developed in the films after thermal treatment were studied by the grazing incidence X-ray diffraction (GIXRD) technique.[19] Data were collected on a Siemens D500 powder diffractometer with a special 0.4° axial soller slit and a flat LiF monochromator at the diffracted beam. A Cu anode operating at 40 kV and 25 mA and a scanning speed of 0.15° min^{-1}, were used. Diffraction patterns of the films were recorded between $2\theta=$ 20 and 50°, with an incident angle of $\alpha=1°$.

Scanning electron microscopy (SEM) images were taken on random locations of the surfaces, in order to characterize the film microstructure. A quantitative description of the structures found is obtained by computerized processing and measurement of those images.[20] An example is shown in Fig. 2. From

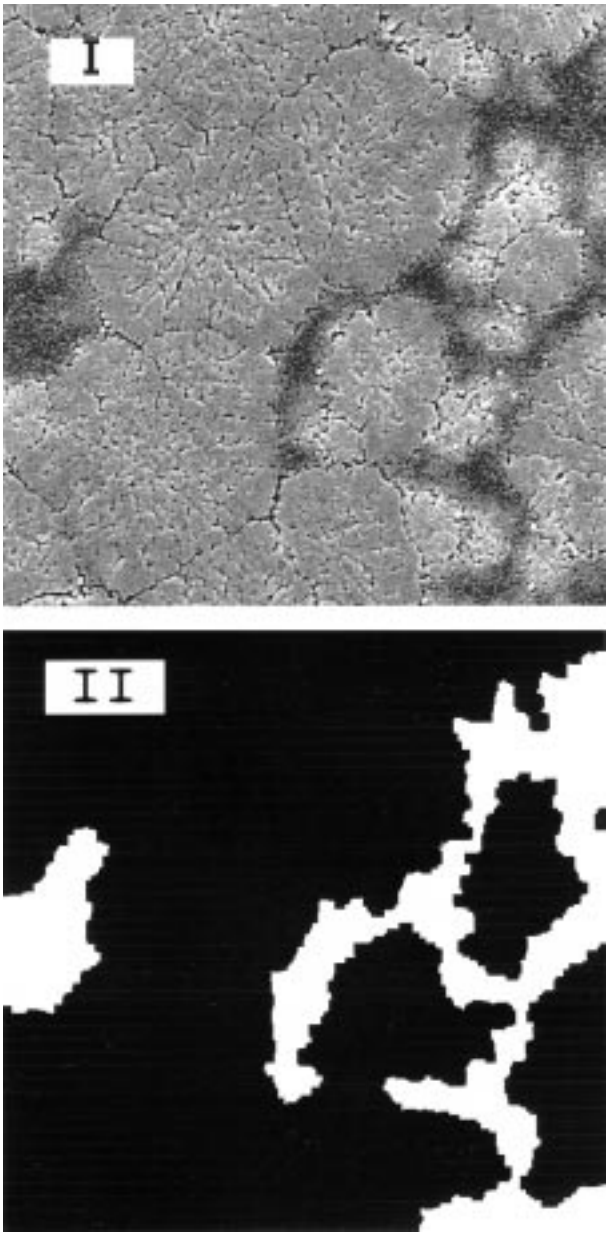

Fig. 2 Image analysis of the SEM micrographs for the measurement of the perovskite content in the films. (I) SEM micrograph, (II) final image in which the relative area of the perovskite rosettes to that of the whole image is calculated

Table 1 Thermal decomposition of the solutions dried at 100 °C for 12 h

	mass% loss (TG)		compounds eliminated[a]	thermal decomposition
T/°C	PTS-A	PTS-B	(EGA)	process
<200	2.99	2.81	H_2O	loss of free water
200–400	17.02	18.26	H_2O, CO_2 (CO)	elimination of bonded water and organic groups
>400	1.98	0.59	H_2O, CO_2	residual organics
total	21.99	21.66		

[a]During decomposition.

the original SEM grey level micrograph [Fig. 2(I)] we obtain a simplified binary image on which measurement takes place [Fig. 2(II)].

Energy dispersive spectroscopy (EDS) was carried out on surfaces of the films. The excitation energy used for the analysis was 30 kV. These studies were made on *ca.* 0.06 μm diameter probe to measure local composition and in a large area of *ca.* 100 μm diameter, to obtain an average composition value. To minimize the interference of the substrate, films with a thickness >1 μm were prepared by multiple coating of the solution on the $Pt/TiO_2/Si$ substrates. ZAF corrections were made on the experimental data to reduce the matrix effect. Lead, titanium and samarium contents were quantitatively measured by analysis of the Pb M-lines, Ti K-lines and Sm L-lines of the experimental spectra. Calibration was performed with samples of the pure elements.

Plane-view specimens for transmission electron microscopy (TEM) were prepared from 3 mm discs, cut from films and mechanically polished from the substrate side to *ca.* 200 μm thickness. Then, they were dimpled and thinned by Ar^+ ion milling at 15°, with a gun current of 0.5 mA and a voltage of 5 kV. Observations were carried out in a Philips CM30 microscope at 300 kV.

Gold electrodes of *ca.* 0.5 mm diameter and *ca.* 35 nm thickness were deposited by sputtering on the top surface of the films to determine their ferroelectric properties. Polarisation-electric field characteristics were evaluated by means of a modified Sawyer–Tower circuit. Hysteresis loops were traced with a sine wave of $V_{max}=10$ V at a frequency of 100 Hz. Resistance (R) and capacitance (C) compensation were carried out using a previous measurement of R and C with a low and non-disturbative voltage.[21,22] The temperature dependence of the dielectric permittivity measured at 1 kHz from room temperature to 500 °C was also studied.

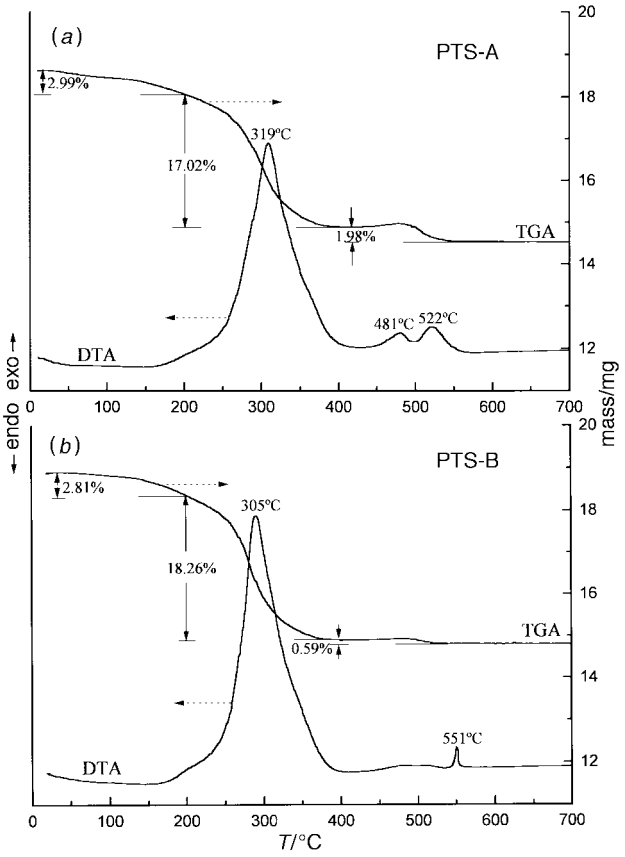

Fig. 3 TGA and DTA curves in air, between 25 and 700 °C and with a heating rate of 10 °C min^{-1}, of (*a*) solution PTS-A and (*b*) solution PTS-B, dried at 100 °C for 12 h

Results

Solutions obtained by these two routes, PTS-A and PTS-B, are precipitate-free and stable in air over many months.

The TGA and DTA curves of Fig. 3(*a*) and (*b*) show the thermal decomposition in air of the PTS-A and PTS-B dried solutions, respectively. Table 1 summarizes the mass losses measured during the thermal analysis of both gels together with the list of the compounds removed in every temperature interval, determined by EGA.

The two types of stoichiometric solution derived powders, after thermal treatment at 700 °C, develop the perovskite phase accompanied by another phase, as can be seen in the XRD patterns of Fig. 4. Similarly, the two types of films contain undesirable phases together with the main perovskite structure, as shown in Fig. 5(*a*) and (*b*) for films crystallized at different temperatures. The XRD patterns of films prepared from PTS-B solutions with an excess of PbO, only show the presence of a randomly oriented perovskite when an excess of PbO of 20 mol% is incorporated (Fig. 6). In contrast, the patterns of the corresponding powders (Fig. 7) indicate a complete disappearance of the second phases with a 10 mol% excess of PbO,

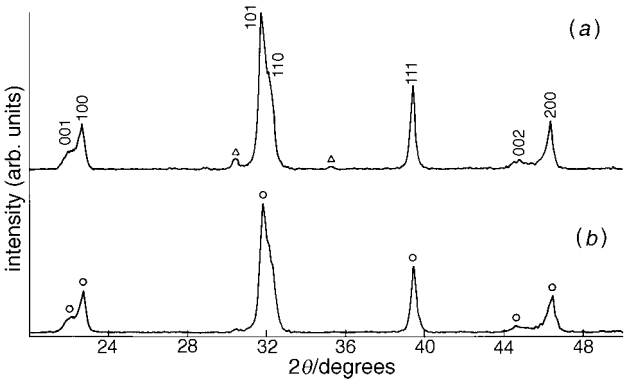

Fig. 4 XRD patterns of samples of solutions PTS-A and PTS-B dried at 100 °C for 12 h and fired at 700 °C for 12 min with a heating rate of 10 °C min^{-1} [○, (Sm, Pb)TiO_3; △, second phases]

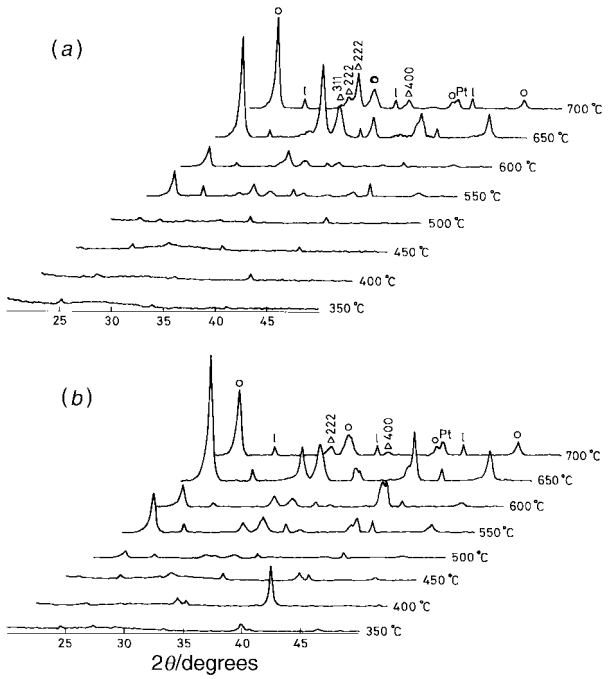

Fig. 5 XRD patterns of films fired at different temperatures for 12 min with a heating rate of 10 °C min^{-1} and deposited from (*a*) solution PTS-A and (*b*) solution PTS-B. l, Laue Bragg peaks corresponding to silicon substrates; ○, (Sm, Pb)TiO_3; △, second phases.

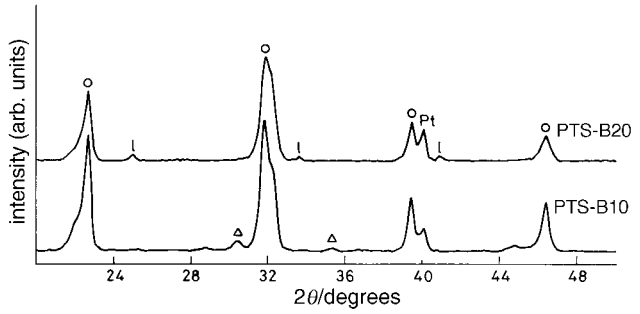

Fig. 6 XRD patterns of films deposited from the solutions PTS-B10 and PTS-B20, and fired at 700 °C (symbols as in Fig. 5)

Table 2 Cell parameters and tetragonal distortion of (Pb,Sm)TiO_3 perovskites developed in films and powders fired at 700 °C and derived from solutions PTS-B with different excesses of PbO

	PbO excess (mol%)	*a*/Å	*c*/Å	*c*/*a*
film	0	3.927	3.994	1.017
	10	3.930	4.032	1.026
	20	3.933	4.017	1.021
powder	0	3.912	4.042	1.033
	10	3.895	4.117	1.057
	20	3.891	4.139	1.064
$Pb_{0.88}Sm_{0.08}TiO_3$ bulk ceramic		3.906	4.074	1.043

whereas the powders prepared with a 20 mol% excess of PbO show a remanent PbO phase together with a well crystallized perovskite.

Table 2 shows the cell parameters of the perovskite from XRD data measured in films and powders derived from PTS-B solutions, stoichiometric and prepared with different PbO excesses.

The thickness of the films, virtually defect-free and showing appropriate adhesion to the Pt substrate, obtained after a single deposition followed by thermal treatment, is *ca.* 0.5 μm (Fig. 8).

The scanning electron micrographs of Fig. 9 show the development of complex microstructures in both PTS-A and PTS-B derived films, consisting of rosette shaped regions surrounded by a fine-grained phase. Under the same thermal treatment conditions, a smaller amount of fine-grained phase is observed in films derived from the solution PTS-B. This fact is clearly shown in the micrographs of Fig. 9(*a*) and (*b*). These microstructures correspond to films PTS-A and PTS-B crystallized at

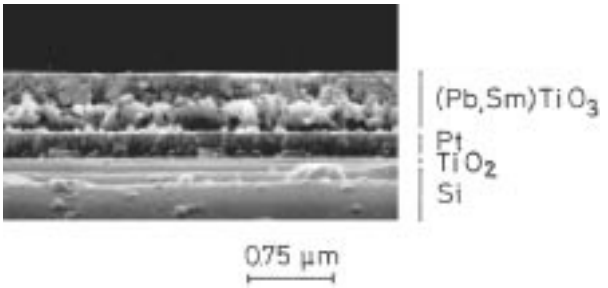

Fig. 8 Cross-section of a single coated samarium modified lead titanate film

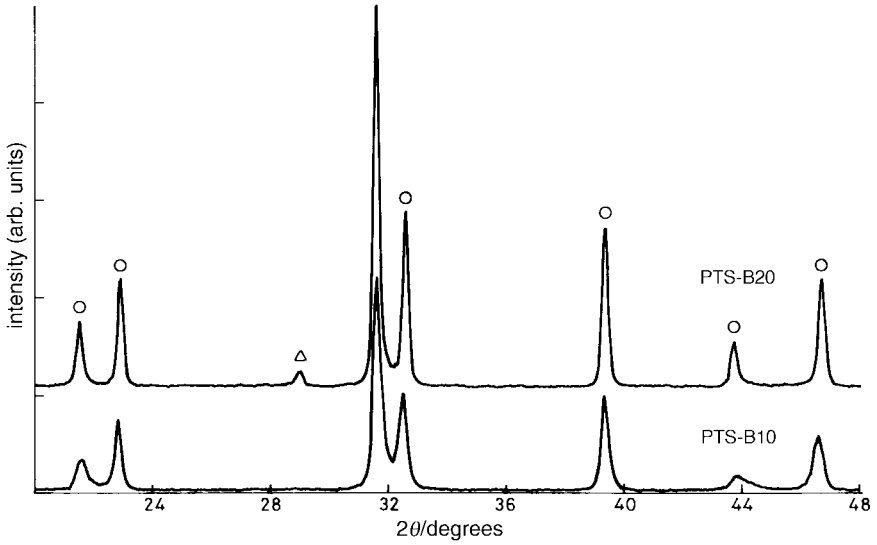

Fig. 7 XRD patterns of powders derived from the gels PTS-B10 and PTS-B20, and fired at 700 °C [○, (Sm,Pb)TiO_3; △, PbO]

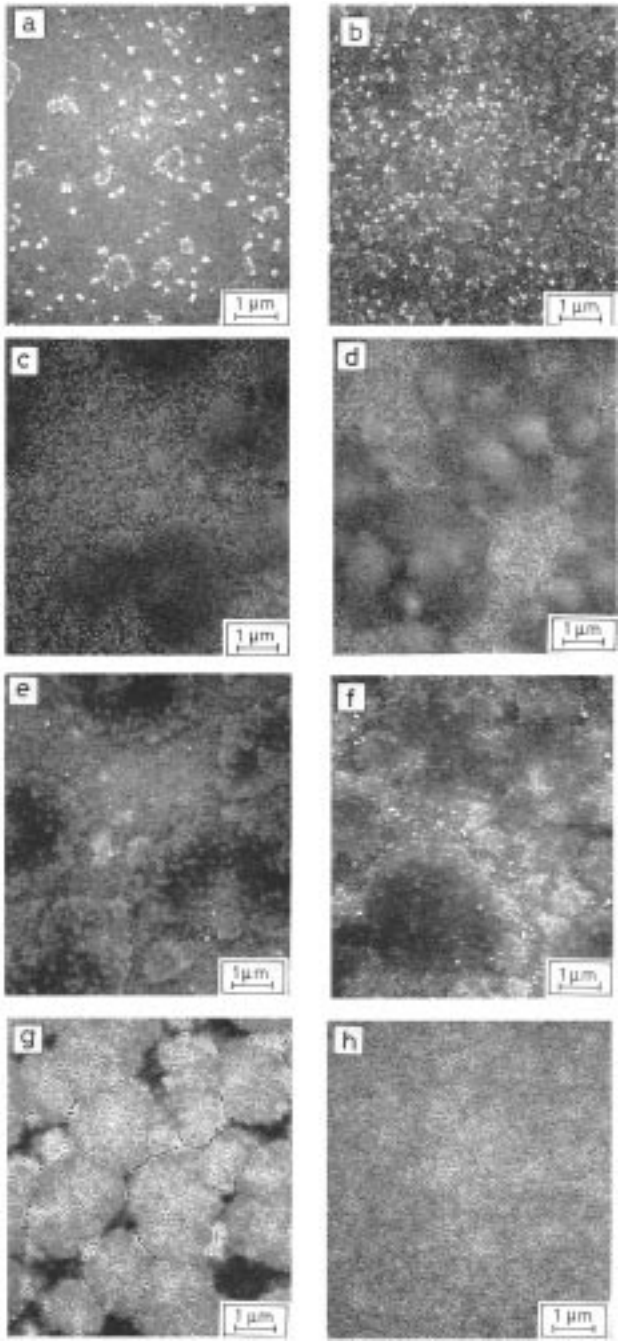

Fig. 9 SEM micrographs of (*a*) film deposited from solution PTS-A and fired at 700 °C for 12 min with a heating rate $\geqslant$500 °C min^{-1}, (*b*) film deposited from solution PTS-B and fired at 700 °C for 12 min with a heating rate $\geqslant$500 °C min^{-1}, (*c*) film deposited from solution PTS-A and fired at 550 °C with a heating rate of 10 °C min^{-1} and a soaking time of 12 min, (*d*) film deposited from solution PTS-B and fired at 550 °C with a heating rate of 10 °C min^{-1} and a soaking time of 12 min, (*e*) film deposited from solution PTS-A and fired at 700 °C with a heating rate of 10 °C min^{-1} and a soaking time of 12 min, (*f*) film deposited from solution PTS-B and fired at 700 °C with a heating rate of 10 °C min^{-1} and a soaking time of 12 min, (*g*) film deposited from solution PTS-B10 and fired at 700 °C with a heating rate of 10 °C min^{-1} and a soaking time of 12 min and (*h*) film deposited from solution PTS-B20 and fired at 700 °C with a heating rate of 10 °C min^{-1} and a soaking time of 12 min

700 °C for 12 min with a rapid heating ($\geqslant$500 °C min^{-1}). Ensembles of crystals embedded in a microcrystalline matrix are observed in both micrographs, but in a larger amount in the films PTS-B. This heterogeneous microstructure, where these ensembles have evolved to form rosette-shaped regions, is also observed when crystallization takes place heating at a 10 °C min^{-1} rate at different temperatures [Fig. 9(*c*)–(*f*)]. The use of PTS-B10 and PTS-B20 solutions, with an excess of PbO, [Fig. 9(*g*) and (*h*)] leads progressively to the formation of films with a more homogeneous microstructure.

The results of the EDS analysis carried out on both the rosettes and the fine grains are shown in Table 3.

Observations by TEM of the films, together with the structural analysis of the different phases by selected area electron diffraction [SAED] are shown in Fig. 10(*a*) and (*b*) for PTS-B films crystallized at 10 °C min^{-1} during 12 min, at 550 and 700 °C. The rosettes show a pattern of a textured ensemble of nanosized single crystals with perovskite type structure. The pattern of the fine-grained phase does not have any preferred orientation. The *d*-spacings measured for this phase are 2.9, 2.5, 1.8 and 1.5 Å.

The variations of the perovskite content of the films, measured as the surface fraction occupied by rosette-shaped regions by computerized image analysis of the SEM micrographs, are shown in Table 4.

A ferroelectric response was not obtained for films deposited from solutions without an excess of lead oxide. On the contrary, hysteresis loops were measurable at 100 Hz in films prepared from solutions with a 10 and 20 mol% excess of PbO (Fig. 11). The variation of the dielectric permittivity with temperature for these films is shown in Fig. 12.

Discussion

Samarium modified lead titanate precursor solutions have been synthesized by a diol-based sol–gel route.[23] Two different methods have been used for the incorporation of samarium to the system. In one of them, samarium acetylacetonate together with titanium and lead reactives are dissolved in propane-1,3-diol, PTS-A [Fig. 1(*a*)]. In the other method, an aqueous solution of samarium acetate is added to a Pb, Ti–propane-1,3-diol sol, PTS-B[16] [Fig. 1(*b*)].

We have reported before how different is the chemistry of diol and water–diol solutions.[24] Obtention of these water–diol solutions is possible because of the capability of the diol-based gels[25] of redissolving in water.[26] Water attacks the polymer network of the gel. As a result, the chemical characteristics of the diol and water–diol solutions are different, affecting the thermal decomposition processes, the microstructure and the final properties of the films.

Three steps can be distinguished in the thermal decomposition processes [Fig. 3(*a*) and (*b*), Table 1] in both systems. An initial mass loss occurs at temperatures below 200 °C and corresponds to the evaporation of water. The subsequent mass loss between 200 and 400 °C is associated with the main exothermic peak in the DTA curves of both systems. The combustion of the majority of the organic compounds is produced in this temperature interval, where H_2O, CO_2 and CO are detected by EGA. It has to be noted that mass losses at these temperatures are larger in the system PTS-B than in the system PTS-A. On the contrary, at higher temperatures, $>$400 °C, a mass loss of *ca.* 1.98% associated with two exothermic peaks at 481 and 522 °C, are recorded in the latter system, while only a *ca.* 0.59 mass% is measured in the former, which is associated with a unique exothermic peak at 511 °C.

Thus, the majority of the volatiles are removed at temperatures below 400 °C for the system PTS-B, whereas higher temperatures are necessary for the system PTS-A. This produces a remaining carbon in the latter that is only removed at high temperatures, close to that of the perovskite crystallization.[27] This thermal evolution can be explained considering the role of water in the PTS-B system that, according to reported results,[24–26] leads to a sol containing simpler polymeric structures than in the PTS-A derived sols. This makes pyrolysis of the polymer easier and thus combustion of organic compounds in the system PTS-B occurs at lower temperatures.

Table 3 Chemical composition of $(Pb,Sm)TiO_3$ thin films measured by EDS

	Pb/Ti molar ratio[a]					
	PTS-A			PTS-B		
PbO excess (%)	rosettes[b]	fine grains[b]	average composition[c]	rosettes[b]	fine grains[b]	average composition[c]
0	0.84 ± 0.02	0.62 ± 0.01	0.75 ± 0.01	0.86 ± 0.02	0.67 ± 0.01	0.83 ± 0.01
10	—	—	—	0.93 ± 0.01	0.91 ± 0.01	0.92 ± 0.01
20	—	—	—	—	—	0.97 ± 0.01

[a]Nominal Pb/Ti ratio = 0.88. [b]Local composition measured on *ca.* 0.06 μm diameter area. [c]Average composition measured on an area of *ca.* 100 μm diameter.

Two features are significantly different between the XRD patterns of the gels and films treated in similar conditions (Fig. 4 and 5): the amount of second phase, developed at temperatures higher than 550 °C, which is higher in the films, and the preferred (100) orientation, also, taking place in the films. These second phases and the orientation of the perovskite tend to disappear progressively as an excess of PbO is incorporated into the precursor solutions (Fig. 6).

Observed differences among the PTS-A and PTS-B derived powders and films are the higher relative intensity of the peaks of the second phase for the materials derived from the PTS-A system, for all the crystallization temperatures tested.

From data in Table 2 another remarkable difference between PTS-B solution derived powders and films is observed. In all the films, lower values of the *c* parameter and higher values of the *a* parameter are measured than for those of the perovskite obtained in $Sm_{0.08}Pb_{0.88}TiO_3$ ceramics.[2] This means that tetragonality of these films is always lower than that of ceramics, as is well known, owing to the strain on the film arising from its interaction with the substrate.[21] Tetragonality of the perovskite crystallized in the stoichiometric powders remains below that of bulk ceramics, whereas, larger tetragonalities than that of the ceramics are measured in powders prepared with an excess of PbO. The tetragonality of the films is always lower than that of the solution derived powders. No remanent PbO is detected in the X-ray patterns of the films prepared with an excess of PbO. However, this phase is observed in the corresponding crystallized powders (Fig. 7). This clearly indicates that volatility of lead is enhanced in the films where the surface to volume ratio is very high.

A complex microstructure is developed in the films derived from stoichiometric solutions as can be seen in Fig. 9(*a*)–(*f*). Studies carried out by TEM on the two microstructural phases of these films, allow us to identify the rosette-shaped textured ensembles of single perovskite crystals of $(Sm,Pb)TiO_3$, surrounded by nanocrystals of a lead deficient phase (Fig. 10). EDS analysis (Table 3) carried out on the rosettes indicates that their composition is close to the nominal composition of the perovskite, $Pb_{0.88}Sm_{0.08}TiO_3$, thus reinforcing the explanation of the low tetragonality measured as due to strain in the film. The EDS analysis of the fine grains indicates that they are deficient in lead with respect to the nominal perovskite composition. Besides, the average composition of the samples seems to indicate a larger deficiency of lead in the films PTS-A than in the films PTS-B, in agreement with the higher content of the second phase detected by XRD. Usually, the structure of these second phases found in materials with similar compositions is regarded as a pyrochlore type.[28,29] Recently, some authors suggested instead a cubic fluorite structure, which matches better with the experimental electron diffraction data obtained for second crystalline phase in PZT.[30–32] The *d*-spacings that we have measured by SAED and XRD, although obtained here for films with different composition, correspond to those of the suggested fluorite structure.

These results indicate that the addition of an excess of PbO to the solutions tends to lead to incorporation into the powders of the perovskite structure, possibly giving rise to a $PbTiO_3$-enriched solid solution. The results also show that the excess of PbO added to the solutions inhibits the formation of the lead deficient second phase and, also, is incorporated into the perovskite to approach the nominal composition, which cannot be reached in films prepared from stoichiometric solutions.

Results of image analysis of SEM micrographs (Table 4) show quantitatively that the content of the second phase is smaller in films deposited from solution PTS-B than in those derived from the solution PTS-A, as XRD and EDS results have already shown. It is also observed that a nearly constant content of perovskite is seen in all the films derived from each system for all annealing temperatures, with the disappearance of the second phase not being observed when using fast firing over short times [Fig. 9(*a*) and (*b*)].[13] These results are in accord with the observations of other authors that lead deficient phases cannot transform into perovskite in films with lead deficiency.[33] Therefore, these films processed from stoichiometric solutions have a considerable content of a second phase, this being larger in the films derived from the diol-solution PTS-A.

Some authors have indicated that the origin of several crystalline phases in addition to the perovskite in sol–gel derived lead zirconate–titanate (PZT) materials is due to a phase separation produced in the precursor solution during the hydrolysis/condensation reactions.[33,34] This could be the cause of the microstructures where perovskite rosettes are embedded in a fine-grained matrix.[12]

These two morphological and crystalline phases are also observed in the $(Pb,Sm)TiO_3$ films of this work. Both seem to appear simultaneously at low temperatures, *ca.* 550 °C (Fig. 5). A larger content of perovskite rosettes is seen in the films PTS-B than in the films PTS-A (Table 4). According to previous work,[33,34] this could indicate a higher homogeneity of the molecular precursor synthesized for the water–diol solution PTS-B than for the diol solution PTS-A. Although, this may be a possible explanation of this phenomenon, it has to be also considered that during the crystallization of the amorphous layers, the combustion of organics leads to a depletion of oxygen in the firing atmosphere. Therefore, formation of a second phase such as oxygen and/or lead deficient pyrochlores or fluorites[30,35] is enhanced in the PTS-A films where organics remain in the material up to temperatures close to the crystallization of the perovskite (Fig. 3 and Table 1).

The formation of (100) oriented rosettes containing microstructures in films deposited on platinized substrates is also explained assuming that (100) perovskite and (111) Pt orientations exhibit the lowest interfacial energy.[36,37] This favours nucleation of oriented nanocrystals at the substrate interface, providing seeds for the crystallization of adjacent amorphous zones. This crystallization mechanism produces the propagation of a radially textured growth,[38] explaining the appearance of star-shaped patterns inside the rosettes [Fig. 9(*g*) and 10].

It has been reported that the transformation of the second phase to perovskite is complete above 550 °C in sol–gel

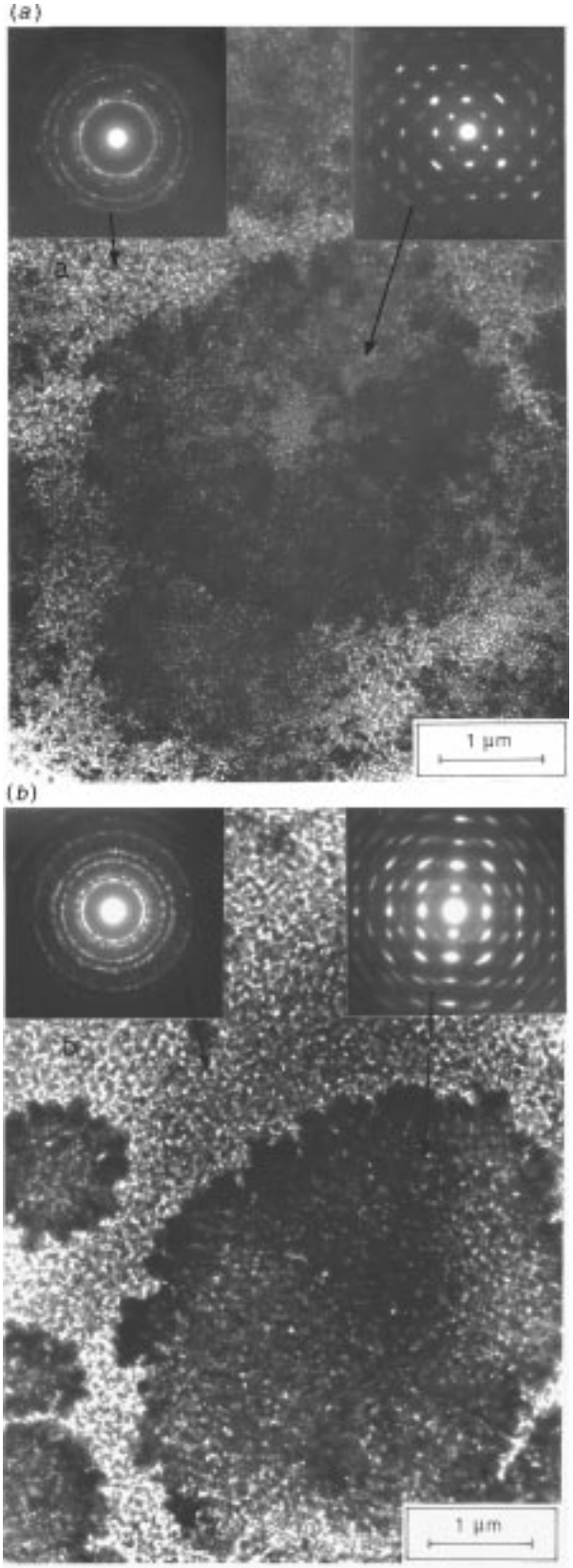

Fig. 10 TEM micrographs and selected area electron diffraction patterns carried out on the rosettes and on the fine grains, of films (*a*) deposited from PTS-B solution and fired at 550 °C, (*b*) deposited from PTS-B solution and fired at 700 °C

lanthanum modified lead titanate films.[39] In $(Pb,Sm)TiO_3$ films deposited from solutions without an excess of PbO, the experimental results do not show an increase in the content of perovskite phase with temperature [Table 4]. On the contrary, the deficiency of lead taking place during crystallization

Table 4 Perovskite content (%) in the films crystallized at 10 °C min^{-1}, obtained from SEM images

T/°C	PTS-A	PTS-B	PTS-B10	PTS-B20
550	51±18	79±7	—	—
650	53±5	65±7	—	—
700	51±5	70±4	83±4	100±0

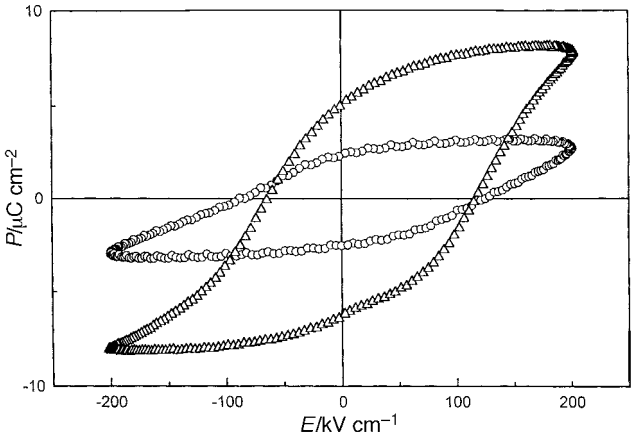

Fig. 11 Hysteresis loops of films fired at 700 °C and deposited from PTS-B10 [10 mol% excess of PbO] and PTS-B20 [20 mol% excess PbO; △] solutions. PTS-B10: $2P_r = 4.8$ μC cm^{-2}, $E_c = 75.8$ kV cm^{-1}; PTS-B20: $2P_r = 11.4$ μC cm^{-2}, $E_c = 89.9$ kV cm^{-1}.

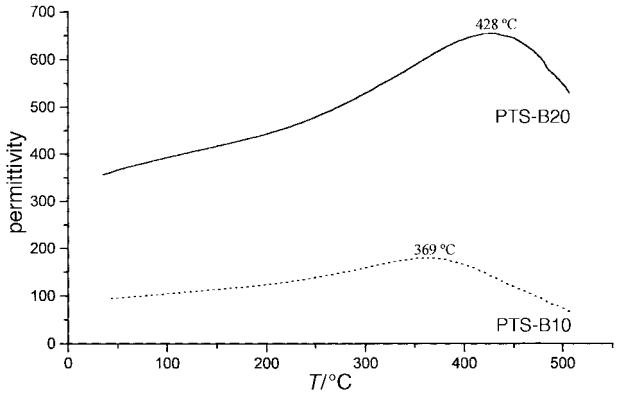

Fig. 12 Permittivity *versus* temperature, (measured at 1 kHz) of films fired at 700 °C and deposited from PTS-B10 [10 mol% excess of PbO] and PTS-B20 [20 mol% excess PbO] solutions

produces more defined rosette boundaries with increase of temperature (Fig. 9 and 10). This may arise from a combination of localized densification owing to crystallization and localized density reductions in the fine-grained phase owing to Pb losses,[40] resulting in a thermal etching effect and in a development of porosity in the second phase.[41] However, the presence of an excess of PbO during crystallization of the perovskite seems to break up the process of (100) oriented nanocrystal nucleation and radial growth, inhibiting the formation of the second phase and causing first, reduction of the rosette size and finally, a disappearance of the rosette microstructure (see evolution in Fig. 9).[42]

A clear ferroelectric response is obtained in films deposited from solutions containing an excess of PbO (Fig. 11). Films derived from solutions without an excess of PbO do not show ferroelectric behaviour, most probably owing to the large amount of secondary non-ferroelectric phases contained in them. According to the XRD and SEM results, films prepared from solutions PTSB-10 (10 mol% excess PbO) still contain a second phase, whereas for films prepared from solutions PTSB-20 (20 mol% excess PbO) only the perovskite is detected by

XRD (Fig. 6). Accordingly, dielectric measurements (Fig. 12) show a significant increase of the permittivity in films with a single perovskite phase (PTSB-20) compared with those that contain fluorite phases (PTSB-10). Also, a displacement towards higher values of the Curie temperature, compared with bulk ceramics of the same composition,[2] at *ca.* 353 °C, is observed in Fig. 12. This is in agreement with the observations of other authors[21,43] who have reported a shift of the transition temperature, together with a decrease of the perovskite tetragonality, although the nominal composition is observed as indicated by EDS results, both arising from the stresses induced by the substrate on the ferroelectric layer.

Conclusions

Ferroelectric samarium modified lead titanate thin films have been processed from diol (PTS-A) and water–diol (PTS-B) solutions with different excesses of PbO. Thermally treated films develop a microstructure of perovskite rosettes composed by sintered grains with a (100) preferred orientation and a fine-grained and porous lead deficient second phase. In addition to the film–substrate interactions, two factors determine the characteristics of these crystallized films: solution chemistry and PbO stoichiometry. Water–diol precursor solutions lead to films with a larger perovskite content than those derived from diol solutions. Further increase of the perovskite content up to virtually 100%, was obtained by using water–diol solutions combined with an appropriate excess of PbO. These latter films have a random orientation, show a homogeneous microstructure and have the highest polarization, as shown by the ferroelectric hysteresis cycle measurements, and the highest dielectric permittivity that have been obtained for films of this composition.

Thanks are due to Dr. E. Snoeck from the CEMES-LOE at Tolouse, France, for his collaboration in the study of samples by transmission electron microscopy, to Drs. M. Kosec and B. Mâlic from the Jozef Stefan Institute of Ljubljana, Slovenia, for their help in the EGA data of the materials and to Dr. P. Ramos for the ferroelectric characterisation of the films.

This work has been supported by projects MAT95-0110 (CICYT-Spain) and CIPA-CT94-023 (EU), and declared to be of technological interest by the EU COST514 action on Ferroelectric Ceramic Thin Films.

References

1 Y. Ito, K. Nagatsuma, H. Takeuchi and S. Jyomura, *J. Appl. Phys*., 1981, **52**, 4479.
2 H. Takeuchi, J. Jyomura, Y. Ito and K. Nagatsuma, *Ferroelectrics*, 1983, **51**, 71.
3 K. Kushida and H. Takeuchi, *Appl. Phys. Lett*., 1987, **50**, 22.
4 H. Takeuchi, *Ceram. Bull*., 1992, **71**, 974.
5 C. F. Millar, W. Wonly, J. Ricote, C. Alemany and L. Pardo, *Br. Ceram. Proc*., 1994, **52**, 185.
6 N. Nagao, T. Takeuchi and K. Iijima, *Jpn. J. Appl. Phys*., 1993, **32**, 4065.
7 G. Teowee, J. M. Boulton, C. D. Baertlein, R. K. Wade and D. R. Uhlmann, *Integr. Ferroelectrics*, 1994, **4**, 231.
8 R. Sirera, M. L. Calzada, J. Ricote and L. Pardo, *J. Sol–Gel Sci. Technol*., 1997, **8**, 425.
9 D. S. Paik, A. V. Prasada Rao and S. Komarneni, *Mater. Res. Bull*., 1997, **32**, 213.
10 L. M. Sheppard, *Ceram. Bull*., 1992, **71**, 85.
11 Y. Xu and J. D. Mackenzie, *Integr. Ferroelectrics*, 1992, **1**, 17.
12 B. A. Tuttle, T. J. Headley, B. C. Bunker, R. W. Schwartz, T. J. Zender, C. L. Hernández, D. C. Goodnow, R. J. Tissot and J. Michael, *J. Mater. Res*., 1992, **7**, 1876.
13 C. C. Hsueh and M. L. McCartney, *J. Mater. Res*., 1991, **6**, 2208.
14 B. A. Tuttle and R. W. Schwartz, *MRS Bulletin*, 1996, **21**, 49.
15 N. J. Phillips, M. L. Calzada and S. J. Milne, *J. Non-Cryst. Solids*, 1992, **147–148**, 285.
16 R. Sirera and M. L. Calzada, *Mater. Res. Bull*., 1995, **30**, 11.
17 H. N. Al-Shareef, K. D. Gifford, S. H. Rou, P. D. Hren, O. Auciello and A. K. Kingon, *Integr. Ferroelectrics*, 1993, **3**, 321.
18 R. D. Klissurka, T. Maeder, K. G. Brooks and N. Setter, *Microelectron. Eng*., 1995, **29**, 297.
19 J. Mendiola, M. L. Calzada, R. Sirera and P. Ramos, *Proceedings of Electroceramics IV*, vol. I, ed. R. Waser, S. Hoffmann, D. Bonnenberg and Ch. Hoffmann. Institut für Wekstoffe der Elektrotechnik (IWE), RWTH Aachen, University of Technology, Germany 1994, p. 327–330.
20 J. Ricote and L. Pardo, *Acta Mater*., 1996, **44**, 1155.
21 J. Mendiola, M. L. Calzada, R. Sirera and P. Ramos, *J. Mater. Sci*., 1996, **31**, 617.
22 M. V. Raymond, J. Chen and D. M. Smyth, *Integr. Ferroelectrics*, 1994, **5**, 73.
23 N. J. Phillips and S. J. Milne, *J. Mater. Sci. Lett*., 1991, **1**, 893.
24 M. L. Calzada, R. Sirera and F. Carmona, *J. Sol–Gel Sci. Technol*., 1997, **8**, 729.
25 M. L. Calzada and R. Sirera, *J. Mater. Sci.-Mater. Electron*., 1996, **7**, 39.
26 C. J. Brinker and G. W. Sherer, in *Sol–Gel Science. The Physics and Chemistry of Sol–Gel Processing*, Academic Press, London, 1990, p. 649.
27 C. Livage, A. Safari and L. C. Klein, *7th International workshop on Glasses and Ceramics from gels*, Paris, France, June 1993.
28 A. H. Carim, B. A. Tuttle, D. H. Doughty and S. L. Martinez, *J. Am. Ceram. Soc*., 1991, **74**, 1455.
29 M. Klee, A. deVeirman, D. J. Taylor and P. K. Larsen, *Integr. Ferroelectrics*, 1994, **4**, 197.
30 M. A. Subramanian, G. Aravamudan and G. V. Subba Rao, *Prog. Solid State Chem*., 1983, **15**, 55.
31 A. P. Wilkinson, J. S. Speck and A. K. Cheetham, *Chem. Mater*., 1994, **6**, 750.
32 C. D. E. Lakeman, Z. Xu and D. A. Payne, *J. Mater. Res*., 1995, **10**, 2042.
33 L. Ma and D. A. Payne, *Chem. Mater*., 1994, **6**, 875.
34 H. K. Chae, D. A. Payne, Z. Xu and L. Ma, *Chem. Mater*., 1994, **6**, 1589.
35 T. Tani and D. A. Payne, *J. Am. Ceram. Soc*., 1994, **77**, 1242.
36 G. R. Fox, S. B. Krupanidhi, K. L. More and L. F. Allard, *J. Mater. Res*., 1992, **7**, 3039.
37 G. R. Fox, S. B. Krupanidhi and K. L. More, *J. Mater. Res*., 1993, **8**, 2191.
38 C. K. Kwok and S. B. Desu, *Ceramic Transactions, Ferroelectric Films*, ed. A. S. Bhalla and K. M. Nair, American Ceramic Society. Westerville, OH, 1991, vol. 25, p. 85.
39 Y. Shimizu, K. R. Udayakumar and L. E. Cross, *J. Am. Ceram. Soc*., 1991, **74**, 3023.
40 M. Huffman, J. P. Goral, M. M. Al-Jassim, A. R. Mason and K. M. Jones, *Thin Solid Films*, 1990, **193/194**, 1017.
41 J. C. Ho, I. N. Lin and K. S. Liu, *J. Mater. Sci*., 1994, **29**, 1884.
42 G. R. Fox and S. B. Drupanidhi, *J. Mater. Res*., 1993, **8**, 2203.
43 G. A. M. Spierings, G. J. M. Dormans, W. G. J. Moors, M. J. E. Ulenaers and P. K. Larsen, *J. Appl. Phys*., 1995, **78**, 1926.

Paper 7/02984E; *Received* 1*st May*, 1997